Report Title: Materials System for Intermediate Temperature Solid Oxide Fuel Cell

Type of Report: Final Technical Report

Reporting Period Start Date: 9/26/02

Reporting Period End Date: 9/25/05

Principal Author(s): Professors Uday B. Pal and Srikanth Gopalan

Dated: January 12, 2006

DOE Award Number: DE-FG26-02NG41539

Department of Manufacturing
15 St. Mary's Street
Boston University, MA 02446

Abstract

The objective of this work was to obtain a stable materials system for intermediate temperature solid oxide fuel cell (SOFC) capable of operating between 600-800^{0}C with a power density greater than 0.2 W/cm^2. The solid electrolyte chosen for this system was $La_{0.9}Sr_{0.1}Ga_{0.8}Mg_{0.2}O_3$, (LSGM). To select the right electrode materials from a group of possible candidate materials, AC complex impedance spectroscopy studies were conducted between 600-800^{0}C on symmetrical cells that employed the LSGM electrolyte. Based on the results of the investigation, LSGM electrolyte supported SOFCs were fabricated with $La_{0.6}Sr_{0.4}Co_{0.8}Fe_{0.2}O_3$-$La_{0.9}Sr_{0.1}Ga_{0.8}Mg_{0.2}O_3$ (LSCF-LSGM) composite cathode and Nickel-$Ce_{0.6}La_{0.4}O_3$ (Ni-LDC) composite anode having a barrier layer of $Ce_{0.6}La_{0.4}O_3$ (LDC) between the LSGM electrolyte and the Ni-LDC anode. Electrical performance and stability of these cells were determined and the electrode polarization behavior as a function of cell current was modeled between 600-800^{0}C. The electrical performance of the anode-supported SOFC was simulated assuming an electrode polarization behavior identical to the LSGM-electrolyte- supported SOFC. The simulated electrical performance indicated that the selected material system would provide a stable cell capable of operating between 600-800^{0}C with a power density between 0.2 to 1 W/cm^2.

Table of Contents

a. List of Graphical Materials and Tables 4

b. List of Tables 5

c. Introduction 6

d. Executive Summary 9

e. Experimental 10

f. Results and Discussions 12

g. Conclusions 18

h. References 19

i. Figures 21

j. Tables 38

List of Graphical Materials

Figure 1. Comparison of conductivities as a function of temperature of various oxygen-ion-conducting solid electrolytes [8].

Figure 2. Temperature dependence of the conductivity of LSGM electrolyte measured using the four-probe technique.

Figure 3. Schematic of the setup employing symmetrical cells for impedance measurements to screen candidate electrode materials.

Figure 4. Schematic of the setup employing LSGM-electrolyte-supported SOFCs for measuring electrical performance.

Figure 5. SEM micrographs of fracture surfaces of cathode/electrolyte interfaces.

Figure 6. A typical impedance plot of an LSGM symmetrical cell with identical electrodes (cathode/anode) at 800°C.

Figure 7. Temperature dependence of the polarization resistance for various cathode materials measured in air.

Figure 8. A plot of interfacial polarization resistance as a function of electrode thickness for symmetrical LSCF/LSGM/LSCF cells measured in air at 800^0C.

Figure 9. Time dependence of ohmic and polarization resistances of symmetrical Ni-GDC/LSGM/Ni-GDC cell measured at 800^0C.

Figure 10. Diffusion profile of lanthanum in the GDC barrier layer as a function of processing temperature.

Figure 11. Time dependence of the interfacial polarization resistances of cermet anodes with and without the LDC barrier layer over LSGM electrolyte at 800^0C.

Figure 12. SEM micrographs of the polished cross sections of the cathodic and anodic sides of the LSGM electrolyte supported SOFC that was electrochemically evaluated. LDC barrier layer was deposited on the anodic side.

Figure 13. Electrical performance of LSGM-electrolyte-supported (1mm thick electrolyte) SOFC with a LDC barrier layer on the anodic side.

Figure 14. Modeling electrode polarization from electrical performance data at 800^0C of LSGM-electrolyte-supported (1mm thick electrolyte) SOFC with a LDC barrier layer on the anodic side.

Figure 15. Stability of the LSGM-electrolyte-supported SOFC with a LDC barrier layer on the anodic side (operating at 800^0C).

Figure 16. Schematic of the desired structure of the anode supported Intermediate Temperature SOFC based on the LSGM electrolyte.

Figure 17. Simulated electrical performance of an anode-supported SOFC based on the LSGM electrolyte (20 μm thick) with a LDC barrier layer on the anodic side.

List of Tables

Table 1. Curve fitting parameters for modeling electrode polarization as a function of electrode thickness.

Table 2. Curve fitting parameters for modeling electrode polarization.

Introduction

Solid oxide fuel cells (SOFCs) are comprised of a layered structure of a dense electrolyte sandwiched between porous and permeable electrodes (anode and cathode). They provide a very attractive and versatile means of efficiently converting chemical to electrical energy from a wide variety of fossil fuels with much lower environmental impact than conventional power generation systems such as those based on gas turbines. In particular, electrical power generation systems based on SOFCs have the following advantages: high power generation efficiency; cogeneration capability; capability of operating on a wide variety of hydrocarbon fuels and generating much lower levels NO_x and SO_x; ability to internally reform hydrocarbon fuels; high power-to-weight ratio; noise-less operation; lower manufacturing time; solid-state structures that can be easily transported; and wide range of applications that include stationary, transportation and military uses. More details are available in [1].

The material property requirements for SOFCs are quite stringent and well established [2-4]. The electrolyte must have adequate oxygen-ion conductivity (>0.03 S/cm), negligible electronic conductivity, be stable in both oxidizing and reducing conditions and remain dense and impervious during cell operation. The porous and gas-permeable electrodes (anode and cathode) must have high electronic conductivity (>170 S/cm) and charge transfer/surface exchange kinetics ($>10^{-7}$ cm/s), be stable in respective gas environments (oxidizing conditions for cathode and reducing for anode) and remain chemically, mechanically and structurally compatible with the electrolyte and interconnect materials. The interconnect (bi-polar separator plate) material that connects the cathode of one cell to the anode of the next cell must be an electronic conductor, remain dense and impervious, be stable in both reducing and oxidizing conditions, and also be chemically, mechanically and structurally compatible with the anode and the cathode materials.

Limitations of the State-of-the-Art SOFCs: The most successful state-of-the-art high-temperature SOFCs are manufactured by Siemens-Westinghouse. They are tubular-cathode-supported SOFCs and operate at 900-1100^{0}C, with fuel utilization of 80-90%, and power density in the range of 0.2-0.5W/cm^2 [5]. The anode, electrolyte, cathode and interconnect materials are Ni-yttria-stabilized ZrO_2 cermet (electronic conductor), oxygen-ion-conducting yttria-stabilized zirconia (YSZ), Sr-doped lanthanum manganite (electronic conductor), and Mg, Ca and Al-doped lanthanum chromite (electronic conductor), respectively. The electrodes (anode and cathode) are 30-40% porous and permit molecular diffusion of gases, and the electrolyte and interconnect are dense. The tubular cathode (1-2 mm thick) is fabricated by green extrusion followed by sintering, the electrolyte (20-40 μm thick) is deposited over the cathode by a plasma spray process, the anode (100-150 μm thick) is slurry coated over the electrolyte followed by sintering, and the interconnect (50-100 μm thick) is deposited over the exposed cathode using a plasma-spray process [5]. The cost of producing fuel-cell stacks with these batch-processed cells is estimated to plateau, with all foreseeable improvements, at $1500/kWe [6]. This is still significantly (an order of magnitude) higher than their gas-turbine counterparts.

Another major difficulty, which presently limits the application of these SOFCs, is its high operating temperature range (900-1100^{0}C). The high temperature makes it necessary to use expensive high-temperature-corrosion-resistant manifolding materials, and high thermal-energy costs are associated with the initial heating of the system.

Although once the cells start operating the heat generated in the process can sustain the temperature. Also, at these high temperatures, when operating the cells at current densities greater than 350 mA/cm^2, there are considerable interfacial reactions that occur at the electrode/electrolyte/interconnect interfaces. It causes cell degradation, and densification of the porous cathode and thus limits the operating life of the cell. Tremendous progress has been made in extending the life of SOFCs operating at 900-1100^{0}C, to more than 16,000 hours with essentially less than 1% degradation in cell performance [7]. Therefore, if the operating temperature of the SOFCs is to be lowered, they must demonstrate similar or superior performance at lower temperature and have longer or comparable operating life. It is possible that a lower operating temperature can increase the operating life of the cells by reducing the interfacial reactions and decreasing the risk of delamination of the cell components during thermal cycling. However, it is not possible to decrease the operating temperature of the present high-temperature SOFC without sacrificing its electrical performance. For instance, a 300^{0}C decrease in the operating temperature from 1000^{0}C causes an order-of-magnitude increase of the zirconia electrolyte resistivity [2]. Therefore, if the operating temperature is lowered from 1000^{0}C to 700^{0}C, an order of magnitude thinner electrolyte will be required to maintain similar ohmic loss. Such a thin electrolyte will cause the cell to lose its mechanical integrity and make it more susceptible to failure during operation. The electrode kinetics has a stronger exponential dependence on temperature and so employing the same electrodes at lower temperatures would result in significant polarization losses, particularly charge-transfer polarization losses at the electrode-electrolyte interfaces. This will drastically reduce the cell efficiency [3]. Hence, if the operating temperature of the SOFC is to be lowered, an entirely new material system for the electrolyte and the electrodes is needed.

It is clear that SOFCs are a very attractive and promising energy conversion technology. However, high processing cost and high operating temperatures are limiting the use of this technology. For commercial viability, there is a need to reduce the fuel cell stack processing cost to not exceed $400/kWe [6]. It is also necessary to identify new electrode-electrolyte materials in order to be able to decrease the operating temperature of the SOFC so that inexpensive manifolding materials can be used and the cost of the initial thermal energy required to heat the cells can be lowered. This work is directed towards the development of a new materials system for the SOFC that can enable lower operating temperatures ((600-800°C).

Choice of Electrolyte Material for the Intermediate-Temperature SOFC: The material selected to function as the electrolyte for the intermediate-temperature SOFC is strontium and magnesium doped lanthanum gallate, $La_{0.9}Sr_{0.1}Ga_{0.8}Mg_{0.2}O_3$, i.e. LSGM. The oxygen-ion conductivity of LSGM, doped ceria, doped bismuth oxide and doped zirconia (YSZ) are compared in Figure 1 [8]. The primary advantage of selecting LSGM as the electrolyte material in this work is its significantly higher oxygen-ion conductivity at lower temperatures compared to the conventional YSZ electrolyte (Figure 1). Oxygen-ion conductivity of LSGM between 500-700^{o}C is 0.04-0.22 S/cm and that of YSZ in the same temperature range is 0.003-0.03 S/cm. Based on the oxygen-ion conductivity criteria, LSGM has more than adequate oxygen-ion conductivity to function as a SOFC electrolyte at temperatures between 600-800^{0}C. Even though Y_2O_3 doped-Bi_2O_3 has a higher conductivity than LSGM (Figure 1), it is unsuitable as an electrolyte material since it is very prone to reduction to metallic Bi in reducing atmospheres and is also mechanically

very fragile [2]. The doped-CeO_2 material does not have as high oxygen-ion conductivity as the LSGM material and is prone to development of small amounts of undesired electronic conductivity on the reducing side (fuel side) of the SOFC [2].
LSGM is very similar to YSZ in terms of its chemical stability. Kim and Yoo [9] have investigated LSGM's stability towards reduction in the P_{O_2} (oxygen partial pressure) range of 0.21 to 10^{-35} atm; conditions relevant to SOFC operation. They have reported that LSGM is stable and has an ionic transference number close to unity (>0.99) under these conditions. It may be noted that undoped $LaGaO_3$ undergoes a first-order phase transition from the orthorhombic to rhombohedral structure [10]. This manifests itself as an abrupt and discontinuous change in the coefficient of thermal expansion at the transformation temperature (400-500^{0}C). However, doping it with Sr on the La sublattice and Mg on the Ga sublattice significantly suppresses this transformation and makes the shrinkage associated with the phase transition negligible [11]. Therefore this phase transition is not of concern for the application of LSGM as an electrolyte. Based on superior oxygen-ion conductivity, negligible electronic conductivity and chemical stability under SOFC operating conditions, LSGM is chosen as the electrolyte material for the intermediate-temperature SOFC.

Choice of Electrode Materials for the Intermediate-Temperature SOFC: This work reports the performance in terms of the polarization resistance of several prospective anode and cathode materials for application in the Intermediate-Temperature (600-800^{o}C) SOFCs employing LSGM electrolyte. However, the performance of a complete cell is described with the best performing cathode and anode materials systems. Cathode materials investigated included Sr-doped lanthanum manganite ($La_{1-x}Sr_xMnO_3$ or LSM), Sr and Fe doped lanthanum cobaltate ($La_{1-x}Sr_xCo_yFe_{1-y}O_3$ or LSCF), and two porous composite electrodes one comprising a two-phase particulate mixture of LSM-LSGM and the other consisting of LSCF-LSGM. These cathode materials have adequate electronic conductivity to function as a cathode [12] but their interfacial polarization resistance as a function of temperature needs to be determined because that is likely to influence their selection for application in the intermediate-temperature SOFCs. The choice of anode materials focused on Ni-doped ceria composites. Nickel is a well-known SOFC anode material, and acts as the fuel side electrocatalyst and current collector. Usually the SOFC anodes are prepared by mixing and sintering NiO and an oxygen-ion-conducting oxide in air, followed by reducing the NiO to Ni under reducing conditions. Use of lanthanum or gadolinium doped ceria as the oxygen-ion-conducting oxide in the anode would buffer the thermal expansion mismatch between the anode and the electrolyte and also result in lowering the charge-transfer polarization due to its mixed-conducting property [13]; La-or-Gd-doped ceria conducts both oxygen ions and electrons. It has been observed that the Ni phase in the anode reacts with the perovskite LSGM phase forming an insulating lanthanum nickelate phase and this also causes the ohmic and anodic polarization resistances to increase with time [14]. In response to this observation the concept of applying a thin (< 5μm) lanthanum or gadolinium doped ceria barrier layer to prevent direct contact and reaction of Ni with the LSGM electrolyte is presented. Since the doped ceria has sufficiently high oxygen-ion conductivity and the barrier layer is thin, it is not expected to increase the ohmic polarization resistance of the cell.

Executive Summary

The objective of the proposed research is to investigate a materials system for intermediate temperature solid oxide fuel cell that is capable of operating between 600-800^{0}C. The electrolyte, anode, and cathode materials in the SOFC system being investigated are based on lanthanum gallate ($La_{1-x}Sr_xGa_{1-y}Mg_yO_{3-\delta}$ or LSGM), nickel-ceria ($Ce_{0.9}Y_{0.1}O_{2-x}$) cermet, and LSGM-lanthanum cobaltite ($La_{0.8}Sr_{0.2}CoO_3$, or LSC) composite, respectively. These material choices are based on their property information available in the literature.

Interfacial polarizations of the candidate electrodes for the $La_{0.9}Sr_{0.1}Ga_{0.8}Mg_{0.2}O_3$ (LSGM) electrolyte have been investigated by Impedance spectroscopy technique. Several cathode materials were investigated. It included strontium-doped lanthanum manganite (LSM), strontium doped lanthanum cobalt iron oxide (LSCF), porous composite electrodes comprising LSM-LSGM and LSCF-LSGM compositions. The polarization resistances of the cathode materials were measured using impedance spectroscopy on symmetric cells as a function of temperature. Based on these measurements, a 50 vol% porous composite of LSCF and LSGM was identified as the best cathode material. The LSCF-LSGM composite cathode has a polarization resistance that is orders of magnitude lower than both conventional LSM and composite LSM-LSGM cathodes, and also slightly lower than the single phase LSCF cathode. Considering the thermal expansion coefficient (TEC) mismatch between the LSCF cathode and LSGM electrolyte, the LSCF-LSGM composite is also preferred over single phase LSCF. Investigations of IT-SOFC cathode materials have also revealed a dependence of polarization resistance on thickness. The polarization of the cathode layer initially decreases sharply with increasing electrode thickness and then levels off asymptotically. The initial decrease of the cathode polarization resistance can be rationalized on the premise that increasing the electrode thickness results in an increase in the number of electrochemical reaction sites. The subsequent leveling off of the polarization resistance is due to the fact that above a certain critical electrode thickness the migration of the oxygen ions from the reaction sites to the electrode/electrolyte interface become rate controlling. Thus, there is a certain critical thickness beyond which the cathodic polarization resistance shows no further decrease with increasing thickness. This critical electrode thickness is a strong function of the microstructure (grain size) and porosity, i.e. finer the microstructure and finer the porosity, smaller the critical thickness. The fabricated cathodes typically have 1μm average grain size and 25% porosity. From our measurements it is clear that a cathode thickness of 40 μm is sufficient to minimize the polarization resistance. The anode materials investigated were Ni-Gadolinium and Ni-Lanthanum doped Ceria (Ni-GDC and Ni-LDC). It was observed that the LSGM electrolyte reacts with the Ni during processing and also at the operating temperature and increases the polarization resistance. A dense buffer layer of LDC between the LSGM electrolyte and the composite anode prevents this interaction and a much lower electrode polarization is observed.

For the purpose of demonstration, LSGM electrolyte supported SOFCs with the most optimum cathode and anode materials system including the barrier layer between the electrolyte and the anode was fabricated and electrochemically evaluated between 600-800^{0}C. The results of the electrolyte-supported SOFC were used to simulate the electrical performance of the anode-supported SOFC with the selected materials system.

Experimental

Powder synthesis: Electrolyte powders of the composition $La_{0.9}Sr_{0.1}Ga_{0.8}Mg_{0.2}O_3$ (LSGM) were prepared by mixing and ball-milling precursors of lanthanum carbonate, strontium carbonate, gallium oxide and magnesium oxide in appropriate stoichiometric ratios and calcining at a temperature of 1200°C for 4 hours in air. The calcined powders were lightly crushed using alumina mortar and pestle and the calcination step was repeated for completing the solid-state reaction. Electrode materials such as $La_{0.9}Sr_{0.1}MnO_3$ (LSM), $La_{0.6}Sr_{0.4}Co_{0.8}Fe_{0.2}O_3$ (LSCF), $Ce_{0.85}Gd_{0.15}O_2$ (GDC) and $Ce_{0.6}La_{0.4}O_2$ (LDC) were also made using the same mixing and calcination techniques. X-ray powder diffraction analysis confirmed the composition, phase and purity of the material. All the synthesized powders (LSGM, LSM, LSCF, GDC, LDC) and NiO powder purchased from Baker were then separately ball-milled in methanol. Laser Scattering Particle Size Distribution Analyzer (Horiba LA-910) was periodically used at different intervals of the ball milling process to determine the particle size and distribution. The ball milling process was stopped when the desired particle size and distribution were obtained.

Conductivity Measurement of LSGM Electrolyte: For verification with literature measurements, the conductivity of the synthesized LSGM electrolyte was measured using a four-probe DC technique. The four-probe method utilizes four electrodes: two current-carrying Pt electrodes on the two ends of the sample and two Pt voltage probes in the middle of the sample. The platinum probes in the middle of the sample measured the voltage drop (V) after applying a DC current (I) through the current-carrying electrodes. This configuration is well known and allows determination of the total electrical conductivity of the sample without including the electrode impedance [15-17]. The measured resistance of the middle section of the sample is:

$$R = \frac{V}{I} \tag{1}$$

and

$$R = \frac{1}{\sigma} \times \frac{L}{S} \tag{2}$$

where L is the length between the two voltage probes, S is the cross section area of the sample. Thus, the conductivity of the LSGM sample

$$\sigma = \frac{I}{V} \times \frac{L}{S} \tag{3}$$

The conductivities of the LSGM electrolyte measured by the four-probe method are shown in Figure 2. These measured conductivities matched well with the previously reported measurements [18-20].

Symmetrical cell fabrication: Calcined and milled LSGM powders at room temperature were die-pressed at 10,000psi pressure into pellets and sintered in air at 1450°C for 4 hours. The sintered LSGM pellets were 1.4 mm thick and 2 cm in diameter. The LSGM pellets were then all finely ground to a uniform 1 mm thickness using diamond-grinding discs. LSM-LSGM, LSCF-LSGM, NiO-GDC, and NiO-LDC composite electrodes were prepared by thoroughly mixing desired amounts of the powders. The electrode powders (LSM, LSM-LSGM, LSCF, LSCF-LSGM, NiO-GDC, and NiO-LDC) were each dispersed in α-terpeniol solvent to form a paste. For the cathode electrodes

(LSM, LSM-LSGM, LSCF, and LSCF-LSGM) and the anode without the barrier layer, the ground LSGM electrolyte pellets were masked with Scotch™ tape to form an outer ring on both sides and the electrode pastes were painted smoothly on the open circular surfaces. The painted LSGM electrolyte pellets were air-dried, masks removed and fired in air at elevated temperature for 2 hours. The firing temperature was 1100°C for all the cathodes and 1200-1300°C for the anodes (i.e. NiO-GDC and Ni-LDC electrode samples). All electrodes had the same effective area of around 1.33cm^2. When GDC or LDC barrier layers were employed between the Ni-doped-ceria composite anode and the LSGM electrolyte, very fine GDC or LDC powders were dispersed in α-terpeniol solvent to form a paste which was painted on both sides of the LSGM electrolyte. They were air dried and sintered at 1200-1300°C and the anodes were then applied following the procedure described earlier. For the cathode materials, two pieces of platinum mesh were co-sintered on both electrode surfaces to act as current collectors. Lead wires of Pt were used to connect the platinum-mesh current collectors to the measuring instrument. For the anode materials, pieces of nickel mesh were pressed over the electrode surfaces and co-sintered in a reducing atmosphere. Nickel lead wires were used to connect the nickel-mesh current collectors to the measuring instrument.

AC impedance characterization: The experimental setup using the symmetrical-cell arrangement is shown in Figure 3. In this setup, the symmetrical cell was exposed to the same oxidizing (cathodic), or reducing (anodic) atmosphere on both sides and a two-probe configuration was used to measure the impedance spectra. During measurement a constant flow rate of air was maintained for experiments involving the cathode materials, and a constant flow rate of forming gas (95% argon-5% hydrogen) bubbled through water at 25°C was maintained for experiments involving the anode materials. The measurements were made by applying a small-amplitude AC voltage (10mV) to the cell and monitoring the response current as a function of the AC frequency (from 1mHz to 65KHz). A plot of the imaginary part of the measured impedance versus the real part reveals details of the individual ohmic and polarization contributions to the total resistance of the cell. Impedance measurements were made in the temperature range of 600-800°C in 50°C increments for all the samples using a Perkin-Elmer potentiostat/galvanostat (model 263A) and Solartron analytical-frequency-response analyzer (model 1250).

The AC impedance measurements were performed on LSCF, LSCF-LSGM, LSM-LSGM, LSM, Ni-GDC, and Ni-LDC electrodes. For the Ni-GDC electrodes, measurements were made with and without the doped ceria (GDC/LDC) barrier layer. The Ni-LDC electrodes were evaluated with the LDC barrier layer. After the measurements, the samples were sectioned, epoxy mounted and polished. Optical microscopy and scanning electron microscopy were used to measure the grain size, porosity and thickness of the electrodes and confirm the consistency of the microstructure. Electron microprobe analysis and wavelength dispersive spectroscopy were also used to determine diffusion profiles of the elements at the interfaces.

Electrochemical characterization: Well-sintered dense LSGM electrolyte discs were ground to 1mm thickness using grinding discs with diamond particles. LDC paste was painted on one side of the LSGM electrolyte and sintered in air at 1300°C for 4 hours to act as the barrier layer between Ni-LDC anode and LSGM electrolyte. NiO-LDC (50% by volume of NiO) composite anode paste was then painted smoothly on the LDC barrier layer surface and sintered in air at 1300°C for 2 hours. After that, the LSCF-LSGM (50%

by volume of LSCF) composite cathode paste was painted on the other side of the LSGM electrolyte and sintered at 1100^{o}C for 2 hours. The effective electrode area of the cell was 1.33cm^{2}, which was used for the current density calculation.

In order to decrease contact resistance at the anode, a Ni mesh was pressed over the anode surface and two separate nickel lead wires (current and voltage lead wires) were used to connect the nickel-mesh current collectors to the measuring instrument. Similarly, on the cathode side, a Pt mesh was sintered to the cathode at 900°C by using a Pt paste (sintering time 1 hour). Two separate lead wires of Pt (current and voltage lead wires) were used to connect the Pt-mesh current collectors to the measuring instrument. The test setup for the LSGM electrolyte supported SOFC is shown in Figure 4. In this setup, gold O-ring was put between the alumina tube and the LSGM electrolyte to seal the anode side. Thick Mica gasket was used on the cathode side as the seal. The assembled test cell was placed in the hot zone of a vertical furnace.

At the beginning of the tests, forming gas (95% Ar, 5% H_2) bubbled through water at room temperature was introduced on the anode side and an airflow was maintained on the cathode side. The temperature was then slowly increased to 800^{o}C. The NiO in the anode of the single cells was reduced by a stepwise replacement of the forming gas with hydrogen. The reduction was complete in 4 hours in the hydrogen gas.

The electrochemical performance was measured between 600^{o}C and 800^{o}C in 50°C intervals. The gas flow rate of hydrogen was 200 ml/min on the anode side and 150 ml/min. of air on the cathode side. All electrochemical data were obtained by DC methods using a Perkin-Elmer potentiostat/galvanostat (model 263A). Electrochemical characterization consisted of measuring the open circuit voltage (OCV) of the cells under SOFC operating conditions. The ratio of the measured OCV to the expected Nernst voltage provided a metric for determining the leak tightness of the cell. The current–voltage characteristics were measured with increasing current load from zero until the voltage dropped below 0.4-0.5V. The electrical performance of these single cells were evaluated from the I-V plots by determining the ohmic loss, and the electrode polarization losses as a function of the cell current. Some experiments were conducted for longer times (5000 minutes) to determine performance stability. At the end of each test, microstructural characterization of the cells were performed. From these measurements, the overall stability and electrical performance of these cells were assessed.

Results and Discussions

Electrode Microstructures: The microstructure of the composite cathode and anode is crucial to achieving high power densities while operating the cell. Fine microstructure, fine connected porosity and well dispersed ionic and electronic conductors are essential for a good electrode exhibiting low charge-transfer or interfacial polarization. It has been shown by Tanner et al. [21-22] that the effective charge-transfer resistance scales as the square root of the grain size of the electrode material. However, there is a limit to the acceptable pore size. When the electrode pore size is comparable to the mean free path of the gases being transported in and out of the electrodes, the cell performance is dominated by concentration (mass-transfer) polarization. To achieve a balance between these two conflicting requirements, graded electrode structures with a finer microstructure and porosity close to the electrolyte and coarser microstructure and larger porosity away

from it needs to be developed for the supporting electrode. For instance, for an anode-supported SOFC, the fine electrode microstructure close to the electrolyte would have a large three-phase-boundary (ionic-electronic-gas) length and facilitate charge-transfer reactions and the coarser microstructure and porosity of the thicker outer anode layer would facilitate gas transport. In this investigation we are focusing our attention on the fine microstructure that is needed at the electrode interface with the electrolyte.

Fractured surfaces of the LSM, LSM-LSGM, LSCF, LSCF-LSGM, Ni-GDC, and Ni-LDC electrodes and their interfaces show that these electrodes have similar microstructures in terms of their interfacial adherence, porosity and grain size. The grain size is on the order of 1-2 μm and the porosity is between 25-35% measured in terms of percentage area of the pore from the micrographs using Adobe Photoshop software. Sample cross sections of the fractured surfaces of various electrode/electrolyte interfaces are shown in Figure 5. Based on the grain size, porosity and thickness (10-60μm) of the electrodes, gas diffusion is not expected to control the interfacial polarization process particularly for small applied potentials that were used for the AC impedance measurements.

Impedance Spectroscopy: A typical impedance plot measured using the symmetrical cell arrangement is shown in Figure 6. For all samples measured in this investigation, a single depressed arc was observed. As discussed elsewhere by previous workers [23-25], the high-frequency intercept of the impedance spectrum gives the ohmic resistance of the cell (R_{ohm}), which includes the resistive contributions of the electrolyte, the two electrodes, the current collectors and the lead wires. The low-frequency intercept gives the total resistance ($R_{ohm} + R_p$), which includes the ohmic resistance of the cell, concentration polarization (or mass transfer polarization) resistance and the effective interfacial polarization resistance (R^{eff}_{redox}). The total polarization resistance of the electrode (R_p) is then extracted by subtracting the high-frequency intercept from the low-frequency intercept on the impedance plot. Given that the electrodes are thin, the amplitude of the applied AC voltage is small (10mV), and the gas flow over the electrode was continuous, it is most likely that the effective interfacial polarization resistance, R^{eff}_{redox}, dominates the polarization resistance for the electrodes, i.e. the concentration polarization is negligibly small and R_p is essentially equal to R^{eff}_{redox}.

Selection of Cathode Material: In order to lower the interfacial polarization it is well known that the electrode needs to be a mixed conductor (have both electronic and oxygen ion conductivities) [4,13]. Since LSM is a p-type semi-conductor [4,26], it is advantageous to provide the oxygen-ion conductivity by mixing it with LSGM. On the other hand, since the LSCF is already a mixed conductor [27], mixing it with LSGM is not expected to significantly lower the interfacial polarization. However, it is to be noted that there is approximately 50% mismatch in thermal expansion coefficient between the LSCF electrode material (19.5×10^{-6}/K) and LSGM electrolyte material (11.6×10^{-6}/K) [11-12]. Therefore from the point of view of lowering the interfacial thermal stresses it is desirable to have a LSCF-LSGM composite electrode as the cathode. To explore these concepts, several cathode materials, LSM, LSCF, LSM-LSGM and LSCF-LSGM composite electrodes were studied for possible application in Intermediate Temperature (IT)-SOFCs based on the LSGM electrolyte. Figure 7 shows a comparison of the polarization resistances of the above cathode materials as a function of temperature measured using impedance spectroscopy on symmetric cells. The polarization resistance is plotted as

inverse resistance versus inverse temperature. From these studies of cathode materials compatible with LSGM electrolyte it was determined that a 50 vol% LSCF-LSGM porous composite would serve as the best cathode material. As can be seen from Figure 7, the composite 50 vol% LSCF-LSGM cathode has an interfacial polarization resistance that is several orders of magnitude lower than the LSM-LSGM composite cathode, although as expected the later is lower than the conventional single-phase LSM electrode. The interfacial polarization resistance of the LSCF-LSGM composite cathode is also slightly lower than the single phase LSCF cathode. In addition, considering the thermal expansion coefficient (TEC) mismatch between the LSCF cathode and LSGM electrolyte, the LSCF-LSGM composite is preferred over the single phase LSCF material. Our investigations of mixed-conducting cathode materials have also revealed a dependence of polarization resistance on electrode thickness. The polarization resistance of LSCF cathode on LSGM electrolyte is shown as a function of thickness in Figure 8. The polarization of the cathode layer initially decreases sharply with increasing electrode thickness and then levels off asymptotically. The experimental results in Figure 8 agree well with the model proposed by Tanner et. al. [21-22].

$$R_P = R_{ct}^{eff} = \frac{LR_{ct}}{\left(\frac{1+\beta}{1+\beta e^{-2\frac{h}{\alpha}}}\right)(1-p)Le^{-\frac{h}{\alpha}} + \left(\frac{1+\beta e^{-\frac{h}{\alpha}}}{1+\beta e^{-2\frac{h}{\alpha}}}\right)\alpha\left(1-e^{-\frac{h}{\alpha}}\right) + pL} \tag{4}$$

where

$$\alpha = \sqrt{\sigma_{O^{2-}} L(1-p)R_{ct}} \qquad \text{and} \qquad \beta = \frac{\sigma_{O^{2-}} R_{ct} - \alpha}{\sigma_{O^{2-}} R_{ct} + \alpha} \tag{5}$$

in which $\sigma_{O^{2-}}$ is the ionic conductivity of the electrode; h is the electrode thickness; p is the porosity of the electrode; L is the grain size of the electrode; R_{ct} is the intrinsic charge transfer resistance given by

$$R_{ct} = \frac{RT}{ZFi_0} \tag{6}$$

Z is the number of electrons participating in the electrode reaction, F is the Faraday constant, R is the gas constant, and T is the temperature.

In fact, R_{ct} is a function of the electrochemical properties of the electrode/electrolyte pair, and also a function of the microstructure features of the electrode. Usually R_{ct} is treated as an empirical parameter, determined experimentally for a given electrocatalyst/electrolyte pair.

It is evident from Figure 8 that increasing the electrode thickness had the effect of decreasing the effective interfacial polarization resistance. Figure 8 shows a fit to the data employing the model developed by Tanner et al. [22]. The fitting parameters are shown in Table 1.

The initial decrease of the cathode polarization resistance can be rationalized on the premise that increasing the electrode thickness results in an increase in the number of

electrochemical reaction sites, i.e. total three-phase boundary length in the case of composite cathodes, or total pore area in the case of mixed ionic-electronic conductors. The subsequent leveling off of the polarization resistance is due to the fact that above a certain critical electrode thickness the migration of the oxygen ions from the reaction sites to the electrode/electrolyte interface become rate controlling. Thus, there is a certain critical thickness beyond which the cathodic polarization resistance shows no further decrease with increasing thickness. This critical electrode thickness has been shown to be a strong function of the microstructure (grain size) and porosity [21-22], i.e. finer the microstructure and finer the porosity, smaller the critical thickness. Based on our cathode microstructure, it is clear that a thickness of 40 μm is sufficient to minimize the interfacial polarization resistance.

Selection of Anode Material: Nickel is a well-known SOFC anode material, and acts as the fuel side electrocatalyst and current collector. GDC is an excellent oxygen-ion conductor, is chemically and mechanically compatible with the LSGM electrolyte and has electronic conductivity under reducing conditions [2,11,28]. Therefore, Ni-GDC cermet is expected to be an effective anode if its reaction with the LSGM electrolyte can be prevented. The reactivity of the Ni-GDC cermet anode with the LSGM electrolyte was studied by using the Ni-GDC/LSGM/Ni-GDC symmetrical cell at 800^{o}C under a reducing atmosphere (H_2-bubbled through 25^{o}C water bath). Both the ohmic and interfacial polarization resistances increased gradually with time, which is shown in Figure 9. These results were used to confirm that this was due to Ni reacting with the LSGM and forming insulating phases (lanthanum nickelates) at elevated temperatures [14]. Therefore the use of a layer of doped ceria between the LSGM electrolyte and Ni-GDC anode to prevent direct contact between the Ni in the anode with the lanthanum in the LSGM electrolyte was investigated.

Ni-GDC electrodes with GDC barrier layer on LSGM electrolyte: It was apparent from the wavelength-dispersive-spectroscopy (WDS) analysis of these samples that the GDC barrier layer allowed lanthanum diffusion from the LSGM electrolytes (Figure 10). Lanthanum diffusion from the LSGM electrolyte into GDC barrier layer leads to the formation of $Ce_{1-x-y}La_xGd_yO_2$ solution in the GDC barrier layer and resistive phases $LaSrLa_3O_7$ or $LaSrGaO_4$ at the LSGM electrolyte interface [29]. The latter significantly increases the ohmic resistance of the cell. By decreasing the sintering temperature of the GDC barrier layer it is possible to decrease the lanthanum diffusion, but this leads to incomplete densification and poor interfacial adherence of the GDC barrier layer to the LSGM electrolyte. This also causes penetration of the Ni-GDC anode slurry into the LSGM electrolyte surface through the porous GDC barrier layer and results in a time-dependent increase of the ohmic and interfacial polarization resistances similar to when the GDC barrier layer was absent. In conclusion, it was determined that the GDC layer did not serve as an effective barrier layer between the LSGM electrolyte and the Ni-GDC composite anode.

Ni-GDC and Ni-LDC electrodes with LDC barrier layer on LSGM electrolyte: Next, lanthanum doped ceria (LDC) was employed as the barrier layer between the LSGM electrolyte and the Ni-composite anode in order to limit or eliminate lanthanum diffusion from the LSGM electrolyte into the barrier layer. The idea was to eliminate the lanthanum chemical potential gradient at the interface that results in lanthanum diffusion. It is to be noted that unlike the LSGM electrolyte which has a perovskite phase, the LDC barrier

layer has a fluorite structure. The Ni in the anode is not expected to react with the lanthanum in the LDC barrier layer as long as the La content in the LDC is below 50mole% in the cationic site [30]. It was observed that, unlike the GDC, when the LDC barrier layer had 40 mole% La in the Ce site and was sintered at 1300°C, there was no detectable La diffusion from the LSGM electrolyte. The 40 mol% Lanthanum doped ceria (LDC) likely has the same La chemical potential as in the LSGM and therefore prevented the La diffusion between LSGM electrolyte and the LDC barrier layer [30-31]. Also since the La content was below 50mole%, it was expected to be stable in contact with the Ni-composite anode. Since LDC was being employed as the barrier layer, it was logical to also investigate Ni-LDC composite along with the Ni-GDC composite anodes. Time dependence of the interfacial polarization resistance at 800°C of the LSGM symmetrical cells with Ni-LDC and Ni-GDC composite electrodes with LDC barrier layer is shown in Figure 11. Also shown in the same figure is the interfacial polarization resistance of the Ni-GDC composite electrode without the barrier layer. The interfacial polarization resistances of both Ni-LDC and Ni-GDC electrodes with LDC barrier layer were stable over a period of two weeks, whereas the interfacial polarization resistance of the Ni-GDC electrode without the LDC barrier layer increased continuously with time due to the reaction between Ni and the lanthanum in the LSGM electrolyte. From the point of view chemical reactivity and thermal expansion coefficients it would be preferable to select Ni-LDC as the composite anode for the LSGM electrolyte with the LDC barrier layer.

Electrochemical Performance of LSGM Electrolyte Supported Cells: Based on the results of the electrode polarization studies, complete LSGM electrolyte supported SOFCs were fabricated for electrochemical evaluation. The cell components had the following dimensions and compositions:

(a) 1 mm thick dense LSGM electrolyte.

(b) dense adherent barrier layer (15 μm) of lanthanum doped ceria (LDC) between the LSGM electrolyte and the anode.

(c) 50% by volume of Ni-LDC composite anode having a thickness of 30-40 μm and porosity of 25-35%.

(d) 50% by volume of LSCF-LSGM composite cathode having a fine microstructure (1-2 μm grains), with a porosity of 25-35% and thickness of 30-40 μm.

The SEM micrographs of the polished cross section of a typical tested LSGM electrolyte supported SOFC are shown in Figure 12. The tested cell had porous electrodes, dense electrolyte and well-bonded cell components. Although the LDC barrier layer was not always fully dense, the porosity appeared closed and it served its purpose.

The open-circuit voltages (OCV) at a given temperature in the tested cell are very close to the Nernst potential determined by the equation

$$OCV = \frac{RT}{4F}\ln\left(\frac{P_{O_2(c)}}{P_{O_2(a)}}\right) \tag{7}$$

where $P_{O_2(c)}$ is the oxygen partial pressure on the cathode side, and is 0.21 atm for air. $P_{O_2(a)}$ is the oxygen partial pressure on the anode side, and fixed by the H_2O to H_2 ratio at a given temperature. The calculated theoretical OCV for the cell at 800°C is 1.116V when hydrogen is bubbled through water at 25°C (3% water vapor). The measured OCV at 800°C was 1.118V, which was very close to the theoretical value. This result indicated

good cell sealing. Shown in Figure 13 is the dependence of the single cell voltages and power densities of the LSGM electrolyte-supported cell as a function of the current densities tested at 600°C, 650°C, 700°C, 750°C and 800°C. The maximum power density ranged from 190mW/cm^2 at 800 C to 30mW/cm^2 at 600°C.

Performance Model for the LSGM Electrolyte Supported Cells: Since the single cell testing were conducted on electrolyte-supported SOFCs, the current densities were not very high (below 500mA/cm^2). Both electrodes (cathode and anode) had high porosity and their thicknesses were small (around 30-50μm), so the concentration polarization was negligible. At higher current densities, the relationship between the cell voltage and current density can be fitted as per the following equation [32]:

$$E_{cell} = OCV - i \times R_{ohm} - (a + b \times \ln i) \quad (8)$$

The experimental data was fitted to the above equation with three parameters, namely, R_{ohm}, a, and b. As seen in Figure 14, equation 8 fitted the experimental data well at 800°C. Similar fittings were obtained at other temperatures. Table 2 gives the parameters R_{ohm}, a, and b corresponding to the curve fitting results at other temperatures (from 650°C to 800°C). R_{ohm}, primarily consists of the ohmic resistances of the electrolyte, anode, cathode, current collectors, and the interfacial resistances between the electrodes and the electrolyte. The electrolyte resistance, R_{el}, can be calculated according to the thickness (1mm) and the ionic conductivity measured by the four-probe method (Figure 2). It can be seen from Table 2, that R_{el} is a major portion of R_{ohm}.

Performance stability: The performance stability of the LSGM electrolyte supported SOFC was evaluated by operating the cell at 800°C starting with 0.72 V and a current density of 350 mA/cm^2. There was an initial 5% decay in the performance but the cell appear to stabilize after 3500 minutes (Figure 15).

Simulated Cell Performance of Anode-supported SOFC Based on the LSGM Electrolyte: Higher power densities can be achieved with anode or cathode supported SOFCs rather than the electrolyte supported SOFC. Such a cell may have the following cell-component dimensions:

(a) 50% by volume of Ni-LDC composite anode having a fine microstructure near the LDC barrier layer and coarser microstructure away from the barrier layer; porosity 25-35%. Since the design is based on an anode-supported cell, the anode can be 1-2 mm thick and the fine microstructure region at least 30-40 μm thick.

(b) a dense adherent barrier layer (5 μm) of lanthanum doped ceria (LDC) between the LSGM electrolyte and the anode.

(c) 10-20 μm thick dense LSGM electrolyte.

(d) 50% by volume of LSCF-LSGM composite cathode having a fine microstructure (1-2 μm grains), porosity of 25-35% and thickness of at least 30-40 μm.

The cell structure is schematically shown in Figure 16. The cell performance of this anode-supported SOFC based on the LSGM electrolyte can be simulated using the experimental results from the tested LSGM electrolyte-supported SOFC, since both cells consist of the same electrolyte and electrode materials. The only difference is the thickness of electrolyte and anode. The thickness of the electrolyte is 1mm for the electrolyte-supported cell, but is 20 μm for the anode-supported cell, while the thickness of the anode is around 30 μm for the electrolyte-supported cell, but is 1-2 mm for the anode-supported

cell. The change in thickness of the electrolyte will only influence the ohmic resistance of the electrolyte, R_{el}, and the changing thickness of anode will only influence the concentration polarization of the cell. The desired anode-supported cell will use a graded electrode structures, i.e., coarser connected porosity away from the electrolyte-electrode interface to facilitate gas transport and finer connected porosity close to the electrolyte-electrode interfaces to aid in the charge-transfer reactions. The ideal anode-supported SOFC is thus expected to have negligible concentration polarization and the electrode polarization behavior should be similar to the electrolyte supported SOFC. Therefore, the difference in the performance of the tested electrolyte-supported cell and the ideal anode-supported cell will be due to the difference in the respective ohmic resistances of the electrolyte. Using the parameters in Table 2 and equation 8, the cell performance of the ideal anode-supported SOFC based on LSGM electrolyte is simulated in Figure 17. Shown in Figure 17 is the dependence of the simulated cell voltages and power densities of the ideal anode-supported LSGM cell as a function of current densities at 650^{o}C, 700°C, 750°C and 800°C. The maximum power density ranges from 927 mW/cm^2 at 800 °C to 239 mW/cm^2 at 650°C.

Conclusions

The Sr and Mg-doped lanthanum gallate (LSGM) offers the combination of highest ionic conductivity and materials stability under SOFC operating conditions. The Cathode and anode materials for application in Intermediate Temperature (600-800^{o}C) SOFCs employing LSGM electrolyte had been studied. The cathode materials studied included, LSM, LSCF, porous composite electrodes comprising LSM-LSGM and LSCF-LSGM. It was found that the 50 vol% porous composite of LSCF-LSGM was the best cathode material for the LSGM electrolyte. The investigation on mixed conducting (ionic-electronic) cathode materials also revealed a dependence of polarization resistance on cathode thickness. The polarization of the cathode layer initially decreased sharply with increasing electrode thickness and then leveled off asymptotically beyond a critical thickness of 40 micrometers. This critical thickness is a function of the electrode microstructure. The fabricated cathodes typically had 1μm average grain size and 30% porosity. Various anode materials were also studied. It was observed that Ni phase in the SOFC anode reacted with the perovskite LSGM phase to form an insulating lanthanum nickelate phase and this also caused the polarization resistance to increase with time. Therefore, the concept of applying a barrier layer to prevent direct contact and reaction of Ni with the LSGM electrolyte was investigated. GDC barrier layer allowed lanthanum diffusion from the LSGM electrolytes. However, LDC appeared to serve as an effective barrier layer between the LSGM electrolyte and the Ni-composite anode, because LDC had the same La chemical potential as in the LSGM, and the Ni in the anode did not react with lanthanum in the LDC barrier layer, which had a fluorite structure. Considering the chemical reactivity and thermal expansion coefficients, the Ni-LDC composite anode with a thin LDC barrier layer is the best anode material systems choice for the LSGM electrolyte.

Based on the cathode and anode materials studied, a LSGM electrolyte supported SOFC was fabricated and electrically evaluated. It consisted of: Ni-GDC anode; LDC barrier layer between the anode and the electrolyte; LSGM electrolyte, and LSCF-LSGM

composite cathode. The cell had a maximum power density of 190mW/cm^2 at 800^{o}C and 30mW/cm^2 at 600°C. The electrochemical performance of the cell was modeled and the model results were used to simulate the performance of an anode supported SOFC. The maximum power density of the simulated anode-supported SOFC based on 20μm thick LSGM electrolyte with a graded electrode structures can reach 927 mW/cm^2 at 800^{o}C and 239 mW/cm^2 at 650°C. This is consistent with our goal of achieving power densities in the range 0.2 to 1 W/cm^2 between 650-800°C.

References

1) S. Srinivasan, R. Mosdale, P. Stevens, and C. Yang, "Fuel Cells, "Reaching the Era of Clean and Efficient Power Generation in the twenty-First Century," *Annual Review of the Energy and the Environment, **24***, Edited by R. H. Socolow, Annual Reviews, Pao Alto, CA, 281 (1999).
2) N. Q. Minh and T. Takahashi, *Science and Technology of Ceramic Fuel Cells*, Elsevier Publishing Company Inc., New York (1995).
3) B. C. H. Steele, *Solid State Ionics,* **75**, 157, (1995).
4) N. Q. Minh, "Ceramic Fuel Cells," *J. Am. Ceram. Soc.,* **76(3)**, 563 (1993).
5) S. C. Singhal, "Recent Progress in Tubular Solid Oxide Fuel Cell Technology," *Solid Oxide Fuel Cells V*, Edited by U. Stimming, S.C. Singhal, H. Tagawa and W. Lehnert, The Electrochemical Society Proceeding Series, Pennington, NJ, 37, (1997).
6) Internet Bulletin of the Solid State Energy Conversion Alliance, NETL, Pittsburgh, PA, *http://www.seca.doe.gov/Publications/seca_related_documents.htm*
7) Simens Westinghouse Brochure on *SureCELL (1996-2001),* Science and Technology Center, 1310 Beulah Road, Pittsburgh, PA 15235-5098.
8) K. Huang, R. S. Tichy, and J. B. Goodenough, *Journal of American Ceramic Society,* **81**, 2565, (1998).
9) J-H.Kim and H-I.Yoo, *Solid State Ionic*s, **140**, 105 (2001).
10) H. Inaba, H. Hayashi, and M. Suzuki, *Solid State Ionics,* **144**, 99 (2001).
11) H. Hayashi, M. Suzuki, and H. Inaba, *Solid State Ionics,* **128**, 131 (2000).
12) A. Petric, P. Huang, F. Tietz, *Solid State Ionics,* **135**, 719 (2000).
13) M. T. Colomer, B. C. H. Steele and J. A. Kilner, *Solid State Ionics*, **147**, 41 (2002).
14) X. Zhang, S. Ohara, R. Maric, H. Okawa, T. Fukui, H. Yoshida, T. Inagaki, K. Miura, *Solid State* Ionics, **133**, 153, (2000).
15) M. Hattori, Y. Takeda, J. -H. Lee, S. Ohara, K. Mukai, T. Fukui, S. Takahashi, Y. Sakaki and A. Nakanishi, *Journal of Power Sources,* **131**, 247 (2004).
16) Wensheng Wang and Anil V. Virkar, *Journal of Power Sources*, **142**, 1 (2005).
17) Jiho Yoo, Chan Young Park and Allan J. Jacobson, *Solid State Ionics,* **175**, 55 (2004).
18) K. Huang and J. B. Goodenough, *Journal of Alloys and Compounds,* **303**, 454 (2000).
19) N. Trofimenko and H. Ullmann, *Solid State Ionics,* **118**, 215 (1999).
20) J. W. Stevenson, T. R. Armstrong, L. R. Pederson, J. Li, C. A. Lewinsohn and S. Baskaran, *Solid State Ionics,* **113**, 571 (1998).
21) C.W. Tanner, K.Z. Fung and A.V. Virkar, *J. Electrochem. Soc.,* **144**, 21 (1997).

22) A.V. Virkar, J.Chen, C.W. Tanner and J.W. Kim, *Solid State Ionics,* **131**, 189 (2000).
23) H. Hu and M. Liu, *Solid State Ionics*, **109**, 259 (1998).
24) S. Wang, X. Lu and M. Liu, *J. of Solid State Electrochemistry*, **6**, 384 (2002).
25) J. R. Macdonald, *Impedance Spectroscopy: Emphasizing Solid Materials and Systems*, Wiley, New York, (1987).
26) N. Q. Minh, *J. Am. Ceram. Soc*., **76**, 563 (1993).
27) L. W. Tai, M. M. Nasrallah, H. U. Anderson, D. M. Sparlin and S. R. Sehlin, *Solid State Ionics*, **76**, 273 (1995).
28) S. Sameshima, T. Ichikawa, M. Kawaminami, and Y. Hirata, *Materials Chemistry and Physics*, **61**, 31 (1999).
29) M. Hrovat, A. Ahmad-Khanlou, Z. Samardzija, and J. Holc, *Materials Research Bulletin*, **34**, 2027 (1999).
30) K. Huang, J. H. Wan, and J. B. Goodenough, *J. Electrochem. Soc.*, **148**, A788 (2001).
31) Y. Matsuzaki and I. Yasuda, *Solid State Ionics*, 152, 463 (2002).
32) Allen J. Bard, Larry R. Faulkner, *Electrochemical Methods: Fundamentals and Applications*, 2nd Edition, John Wiley & Sons, Inc, NY (2001).

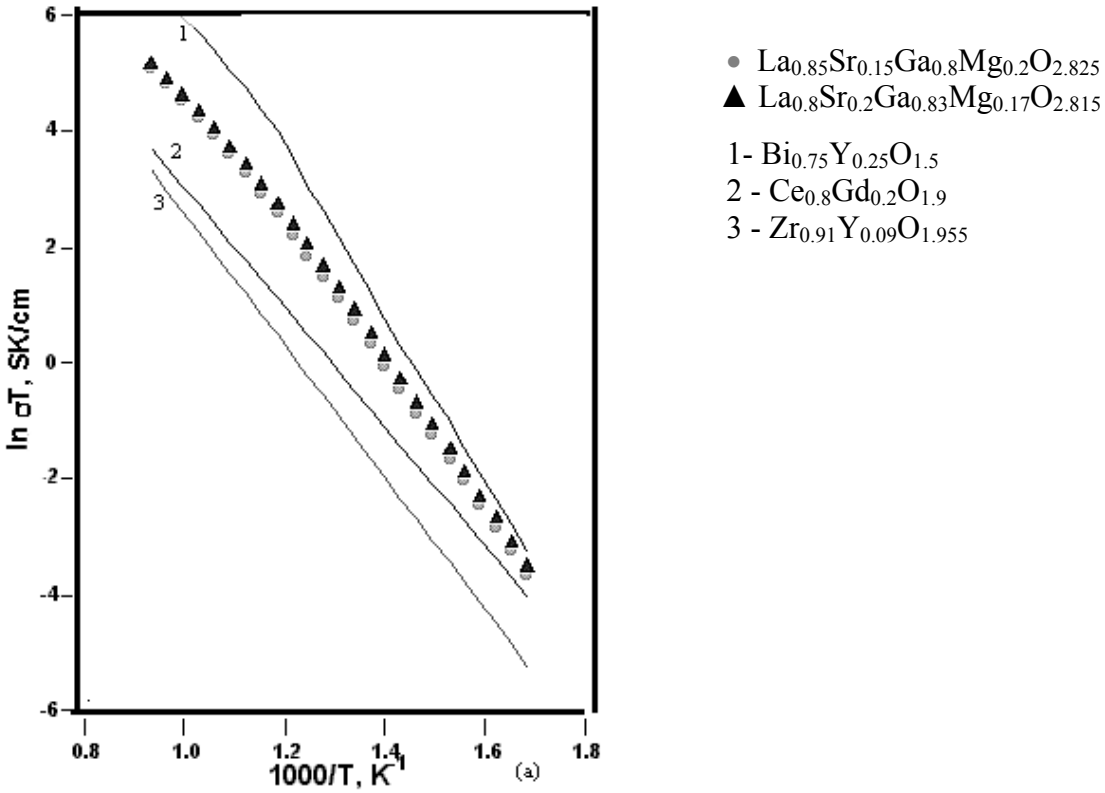

Figure 1. Comparison of conductivities as a function of temperature of various oxygen-ion-conducting solid electrolytes [8]

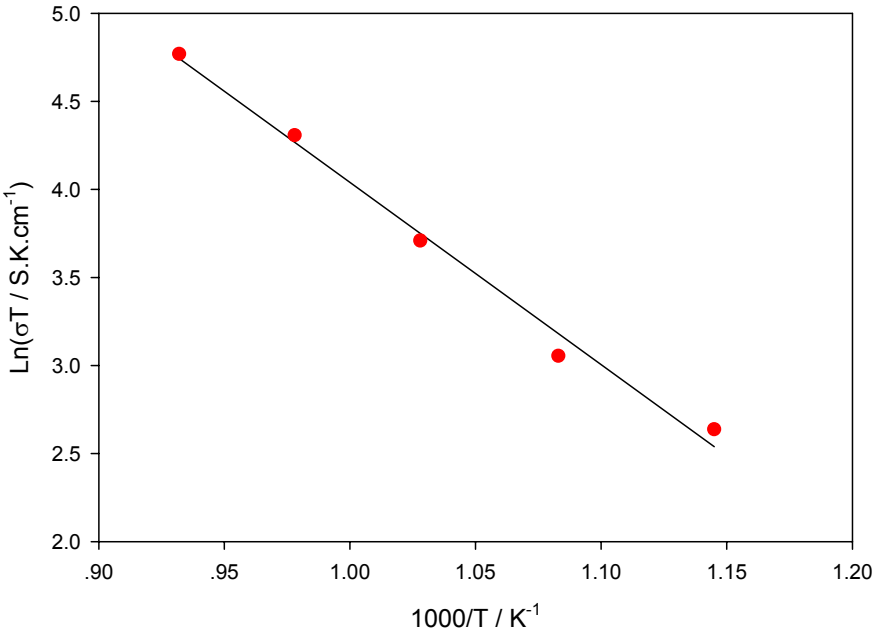

Figure 2. Temperature dependence of the conductivity of LSGM electrolyte measured using the four-probe technique

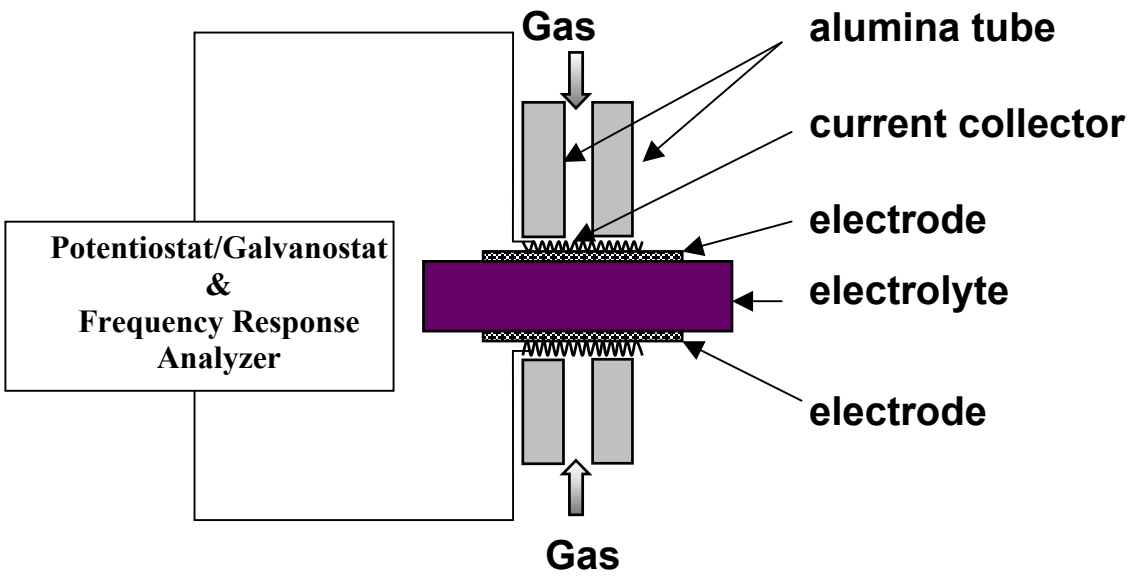

Figure 3. Schematic of the setup employing symmetrical cells for impedance measurements to screen candidate electrode materials

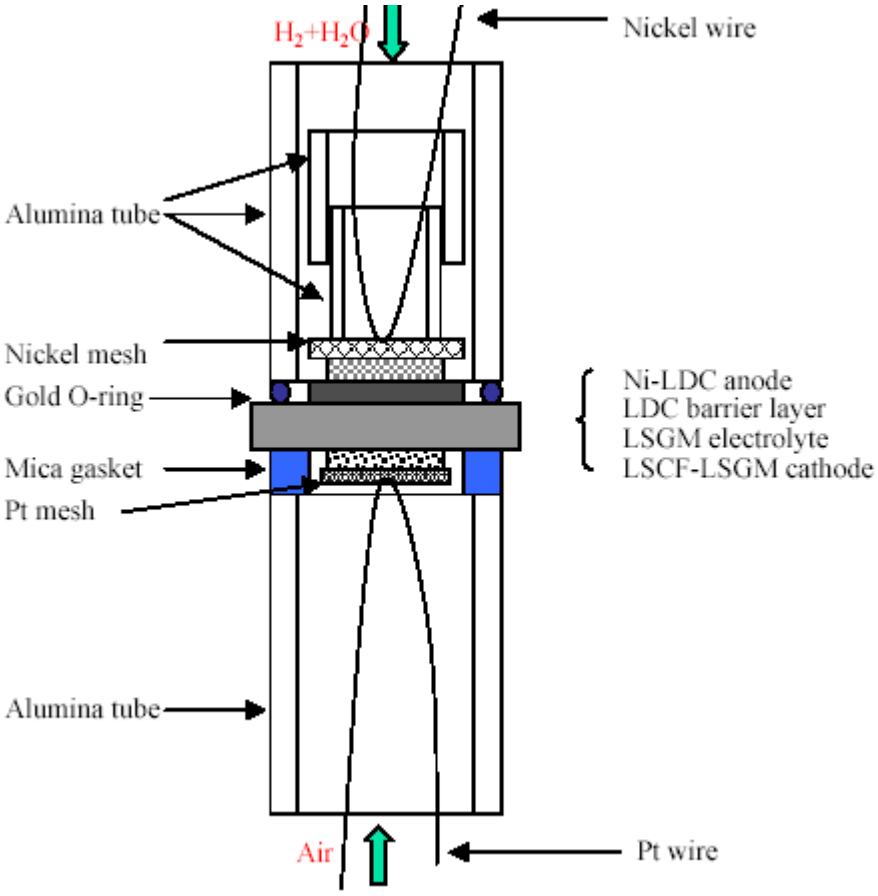

Figure 4. Schematic of the setup employing LSGM-electrolyte-supported SOFCs for measuring electrical performance

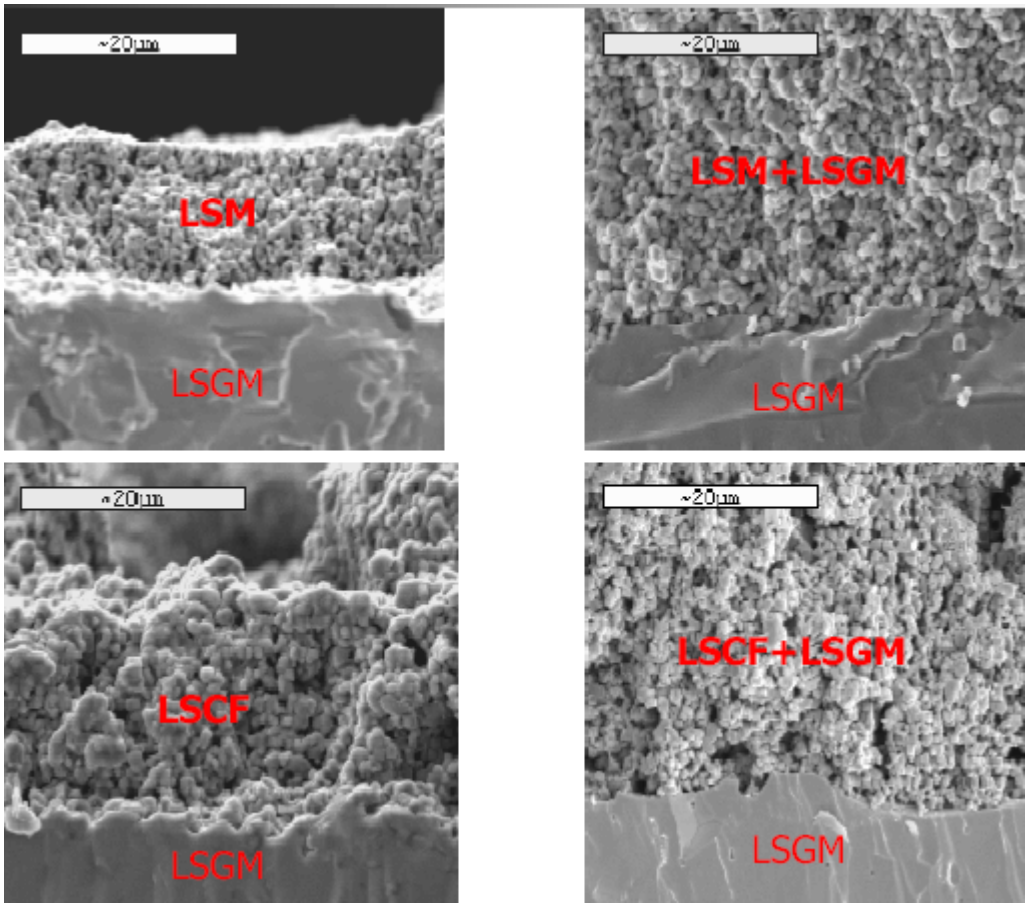

Figure 5. SEM micrographs of fracture surfaces of cathode/electrolyte interfaces

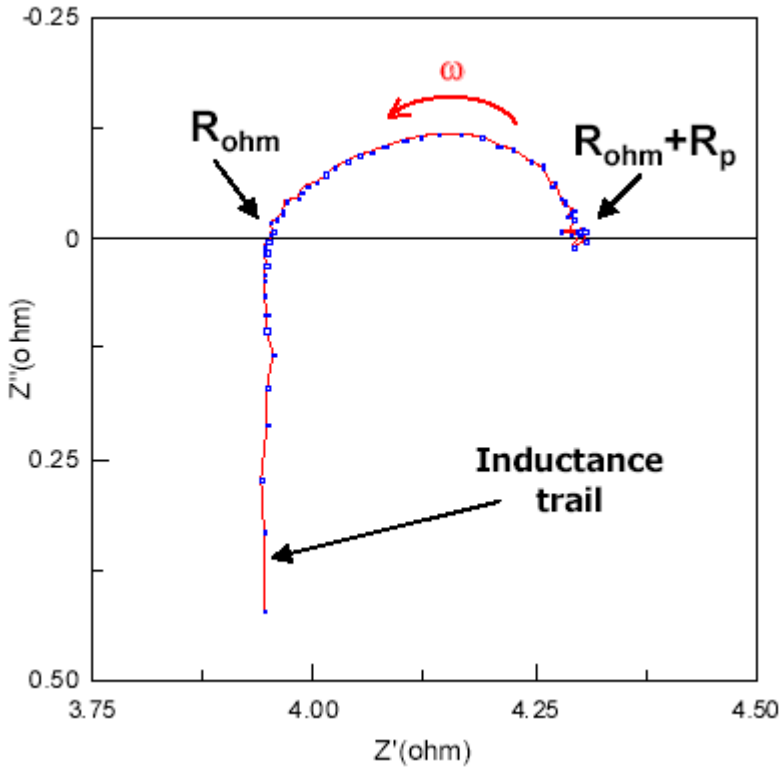

Figure 6. A typical impedance plot of an LSGM symmetrical cell with identical electrodes (cathode/anode) at 800°C

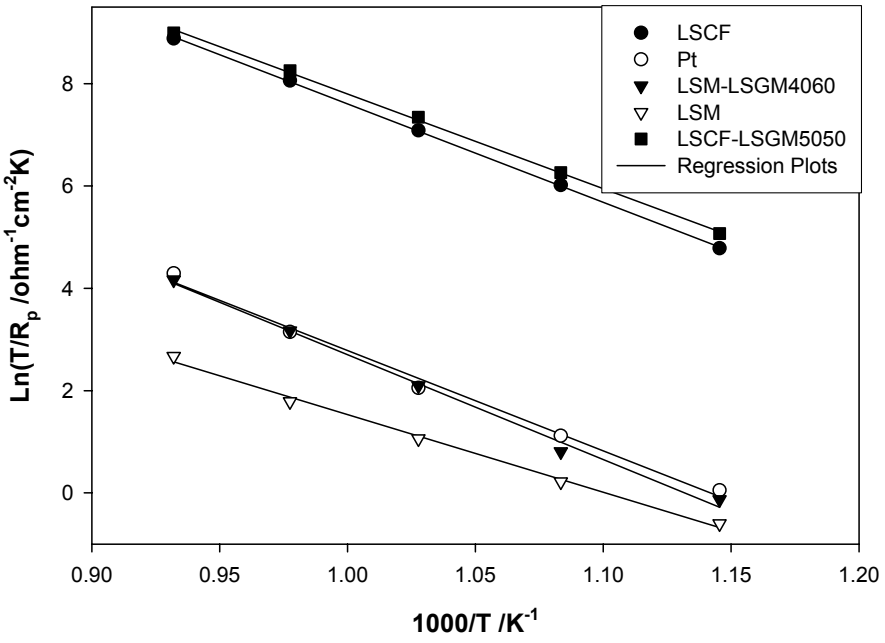

Figure 7. Temperature dependence of the polarization resistance for various cathode materials measured in air

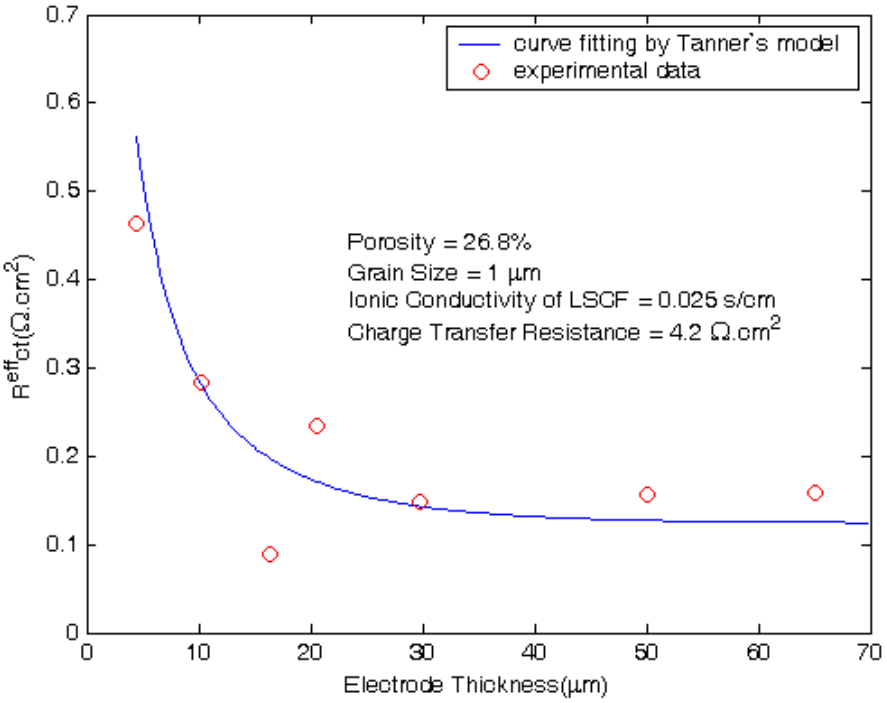

Figure 8. A plot of interfacial polarization resistance as a function of electrode thickness for symmetrical LSCF/LSGM/LSCF cells measured in air at 800^0C

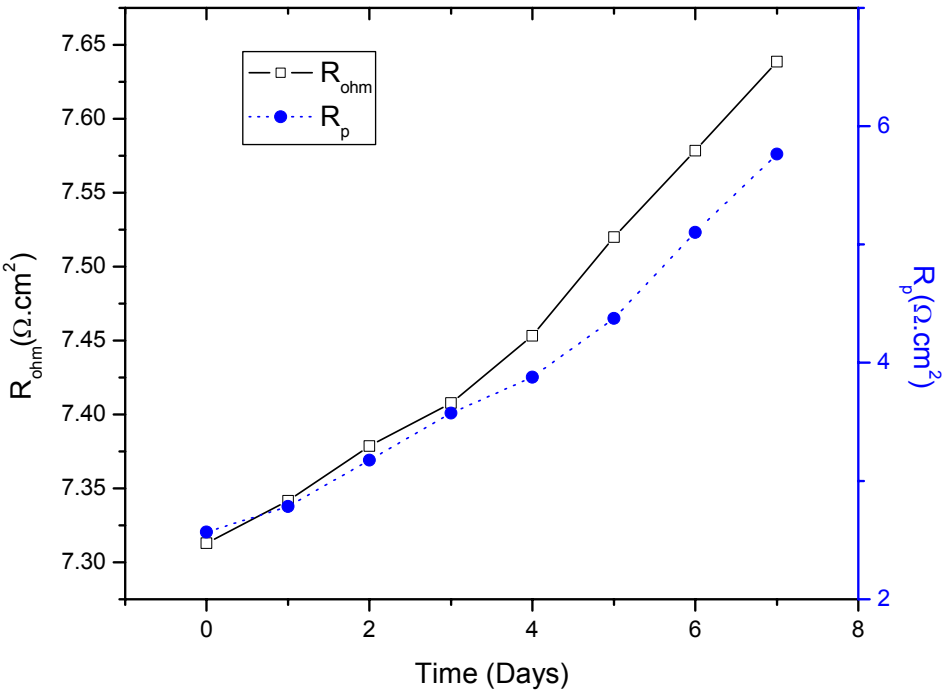

Figure 9. Time dependence of ohmic and polarization resistances of symmetrical Ni-GDC/LSGM/Ni-GDC cell measured at 800^0C

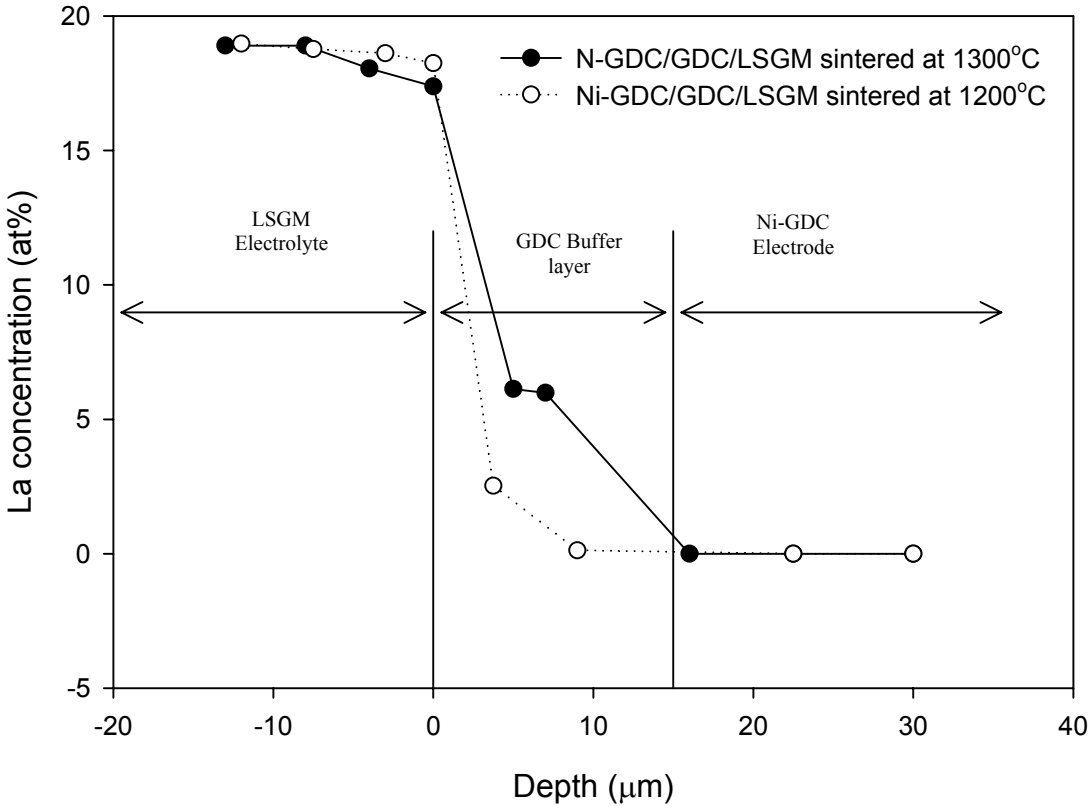

Figure 10. Diffusion profile of lanthanum in the GDC barrier layer as a function of processing temperature

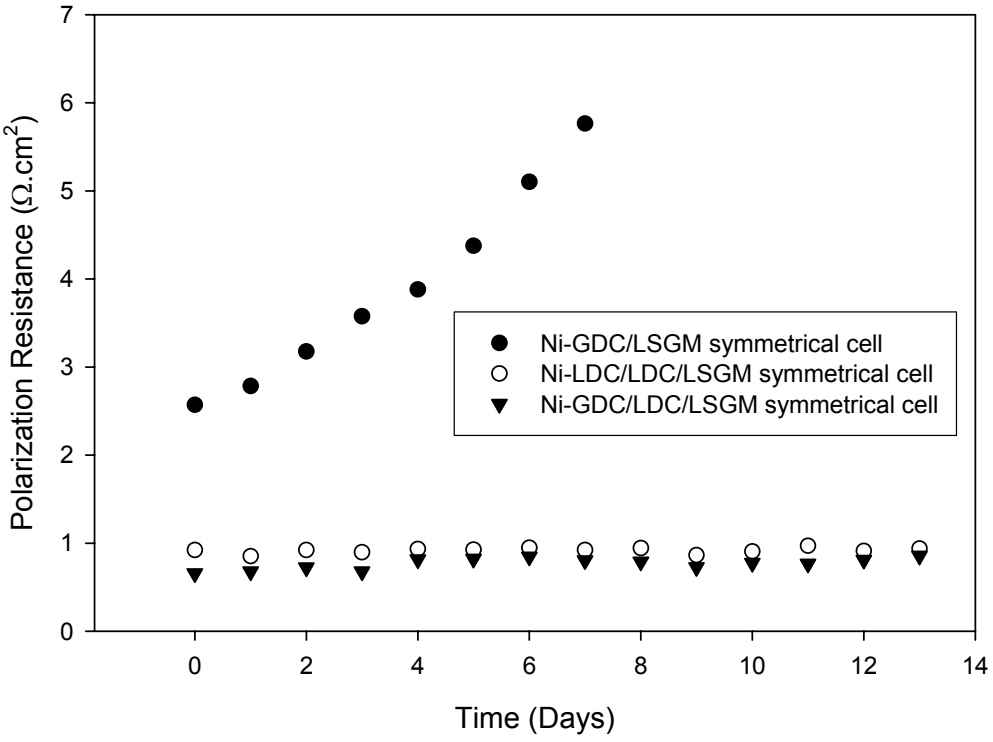

Figure 11. Time dependence of the interfacial polarization resistances of cermet anodes with and without the LDC barrier layer over LSGM electrolyte at 800^0C

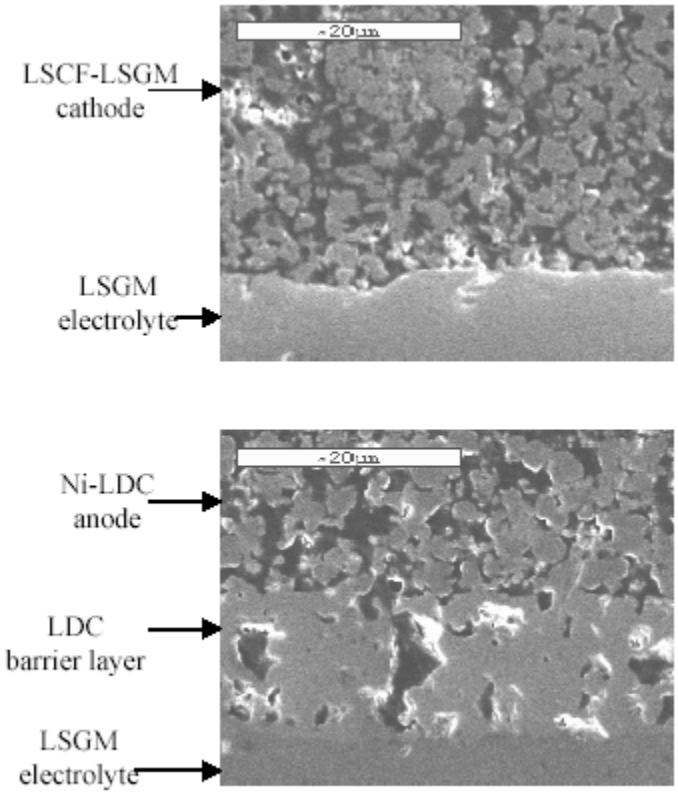

Figure 12. SEM micrographs of the polished cross sections of the cathodic and anodic sides of the LSGM electrolyte supported SOFC that was electrochemically evaluated. LDC barrier layer was deposited on the anodic side

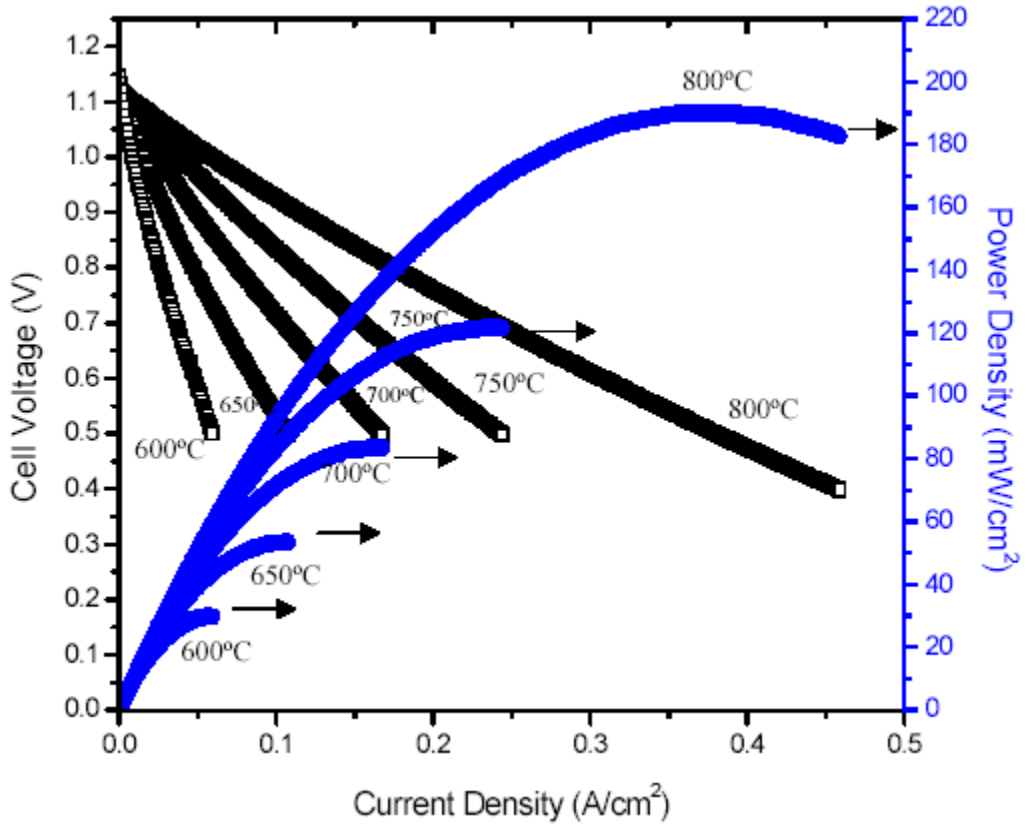

Figure 13. Electrical performance of LSGM-electrolyte-supported (1mm thick electrolyte) SOFC with a LDC barrier layer on the anodic side

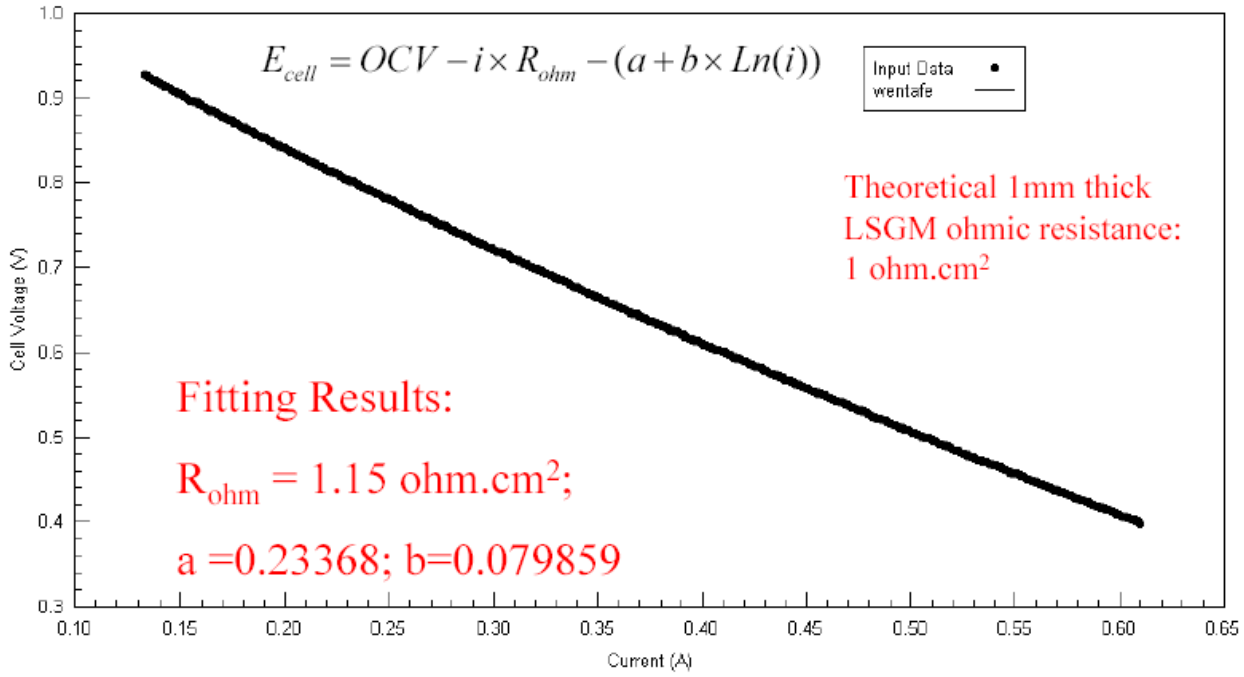

Figure 14. Modeling electrode polarization from electrical performance data at 800^0C of LSGM-electrolyte-supported (1mm thick electrolyte) SOFC with a LDC barrier layer on the anodic side.

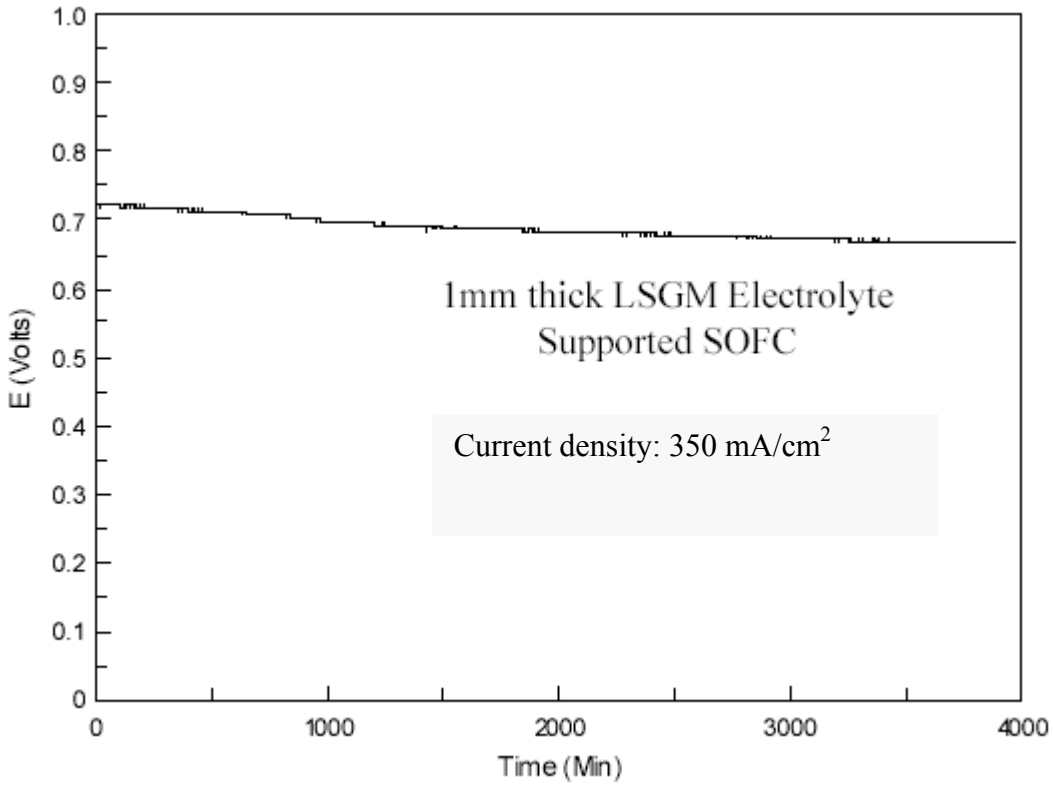

Figure 15. Stability of the LSGM-electrolyte-supported SOFC with a LDC barrier layer on the anodic side (operating at 800^0C)

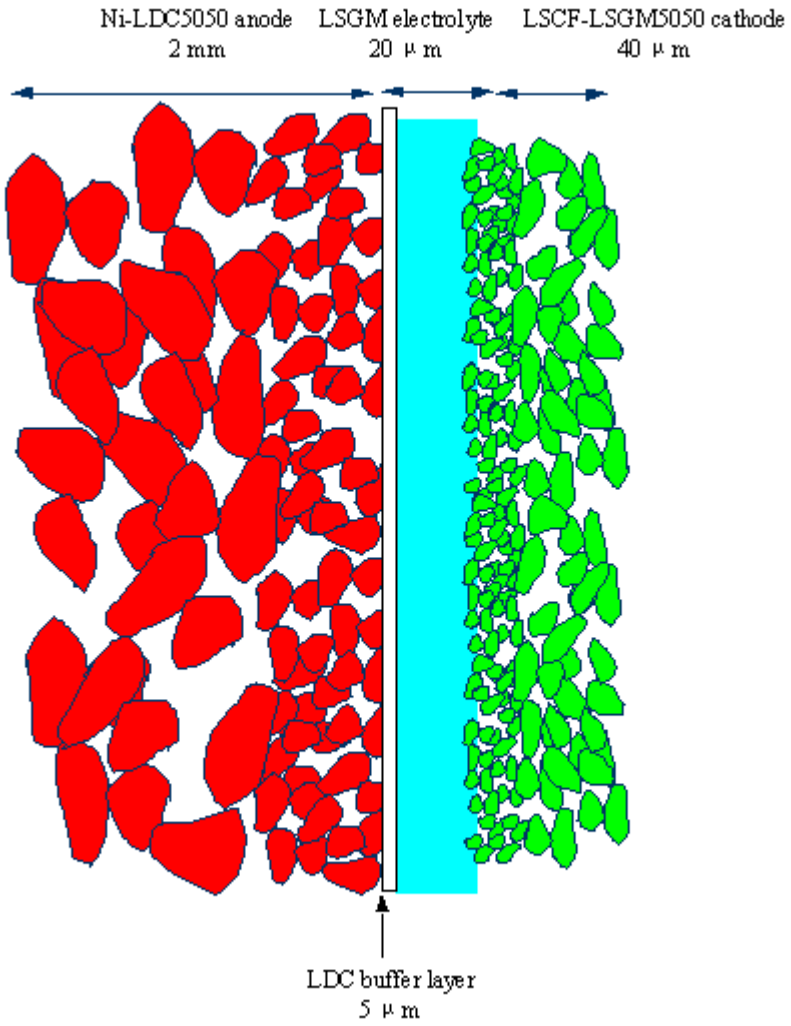

Figure 16. Schematic of the desired structure of the anode supported Intermediate Temperature SOFC based on the LSGM electrolyte.

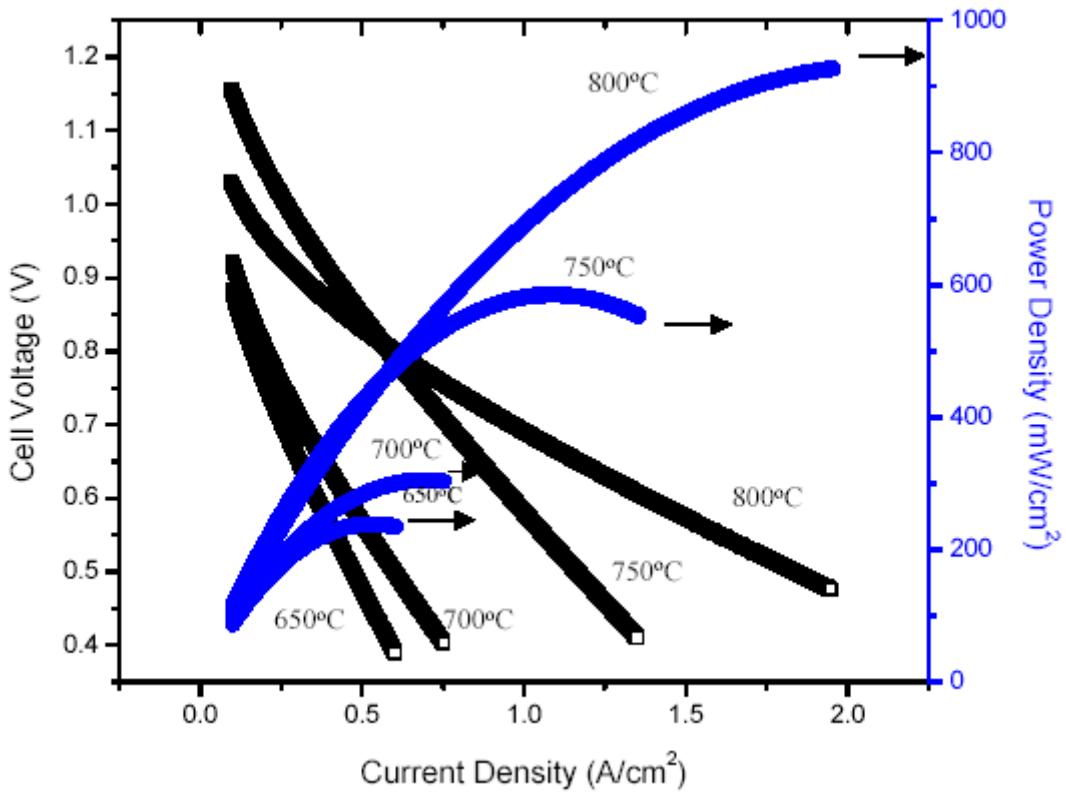

Figure 17. Simulated electrical performance of an anode-supported SOFC based on the LSGM electrolyte (20 μm thick) with a LDC barrier layer on the anodic side.

Table 1. Curve fitting parameters for modeling electrode polarization as a function of electrode thickness.

$\sigma_{O^{2-}}$ (s/cm)	L (μm)	p	R_{ct} ($\Omega.cm^2$)
0.025	1	26.8%	4.2

Table 2. Curve fitting parameters for modeling electrode polarization.

Temperature	R_{ohm} ($\Omega.cm^2$)	a	b	R_{el} ($\Omega.cm^2$)
800°C	1.148	0.23368	0.07986	1
750°C	1.8	0.2795	0.08777	1.43
700°C	2.45	0.3566	0.0988	2
650°C	3.972	0.3415	0.07666	3.353